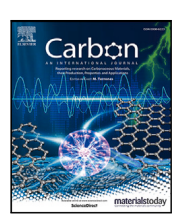


Contents lists available at ScienceDirect

Carbon

journal homepage: www.elsevier.com/locate/carbon



Research paper

MOCVD of WSe2 crystals on highly crystalline single- and multi-layer CVD graphene

Benjamin Huet a,b,c,* , Saiphaneendra Bachu b , Nasim Alem a,b , David W. Snyder c , Joan M. Redwing a,b

- a 2D Crystal Consortium Materials Innovation Platform, Materials Research Institute, The Pennsylvania State University, University Park, PA 16802, United States
- b Department of Materials Science and Engineering, The Pennsylvania State University, University Park, PA 16802, United States
- ^c Applied Research Laboratory (ARL), The Pennsylvania State University, University Park, PA 16802, United States

ARTICLE INFO

Keywords: Graphene Tungsten Diselenide Heterostructure Multilayer Van der Waals Epitaxy

ABSTRACT

The scalable synthesis of van der Waals vertical heterostructures (vdWHs) is viewed as an important milestone for the fabrication of novel 2D-based functional applications. Combining semi-metallic graphene with semiconducting transition metal dichalcogenides (TMDs) shows great potential to explore new device architectures with unique functionalities. In this work, we investigate the gas-source metal-organic chemical vapor deposition (MOCVD) of tungsten selenide (WSe₂) on highly crystalline CVD graphene. Single- and multilayer graphene constitute interesting testing grounds for investigating fundamental WSe₂ growth mechanisms owing to its atomically smooth surface, absence of dangling bonds, chemical inertness, and hexagonal lattice symmetry. Our experimental results show how the graphene template properties influence the WSe₂ nucleation site density, growth rate, in-plane orientation, and thickness. In particular, we found that WSe₂ growth behavior strongly depends on the number of graphene layers, their stacking order/twisting angle, as well as on the nature of the substrate underneath.

1. Introduction

Over the last 15 years, the scientific community has devoted a great deal of efforts to isolate, synthesize, and characterize two-dimensional (2D) materials such as graphene, hexagonal boron nitride (h-BN) and transition metal dichalcogenides (TMDs) [1,2]. These 2D materials offer a wide variety of physical properties that can be harvested in many applications such as transistors [3,4], photodetectors [5,6], solar cells [7], and light emitting diodes [8]. As the field matures in the production of highly crystalline 2D materials, a growing interest is directed towards growing 2D materials on top of each other to form vertical heterostructures [2,9]. Owing to van der Waals (vdW) forces, these artificial stacks can exist in a stable form, regardless of the relative in-plane orientation or the lattice mismatch [10]. Combining 2D materials represents a promising route to engineer the physical properties, improve the performances of 2D based devices, and explore new scientific and technological opportunities [11–14].

To fully realize the potential of 2D-based heterostructures, it is crucial to control the (i) 2D layer sequence, (ii) stacking order or twist angle, (iii) interfacial cleanliness, and (iv) crystallinity and structural quality [15]. Developing a scalable and reliable layer-by-layer

deposition method is also of particular interest when considering the very large scale integration (VLSI) of these heterostructures into future technologies [2]. In this concern, the direct chemical vapor deposition (CVD) of TMDs on graphene represents an ideal approach as it is a fairly scalable process and it offers a clean and sharp interface compared to manual layer-by-layer transfer/assembling processes reported in the literature [16–18].

Over the last 6 years, quite a few studies successfully employed graphene as synthesis substrate for the deposition of TMDs including WSe $_2$ [12,19–22], WS $_2$ [7,23–26], and MoS $_2$ [22,27–30]. Unfortunately, most graphene/TMDs heterostructure growth efforts were based on the in-situ vaporization and transport of solid precursors such as S, Se, MoO $_3$, and WO $_3$ powders. These approaches typically pose several challenges, especially in terms of (i) coverage uniformity, (ii) control over the chalcogen-to-metal ratio and precursor flux, and (iii) growth result dependency on the reactor geometry which drastically hinders the scalability. These limitations can however be overcome by using fully gas-source CVD processes which rely on metal carbonyls (e.g. W(CO) $_6$ and Mo(CO) $_6$) located in bubblers upstream the reactor

E-mail address: benjamin.huetb@gmail.com (B. Huet).

^{*} Corresponding author at: 2D Crystal Consortium Materials Innovation Platform, Materials Research Institute, The Pennsylvania State University, University Park, PA 16802, United States.

and chalcogen hydrides stored in gas cylinders (e.g. $\rm H_2Se, \, H_2S)$ [31–33].

Various sources of graphene have been employed for the synthesis of TMDs including exfoliated graphene from graphite [27,29,34], epitaxial graphene (EG) grown on silicon carbide (SiC) [19-21,23,24,28, 30], or graphene grown on metal catalyst by CVD [12,20,22,23,25,26]. Although EG intrinsically offers a superior surface cleanliness, CVD graphene constitutes a more versatile and compelling substrate for the study of growth mechanisms. Indeed, the CVD of graphene is a cost-effective and industrially viable technique offering large areas of single-layer highly-crystalline material [35-37]. Large crystalline Bernal stacked multilayer (AB-ML) and twisted multilayer (t-ML) domains can also be produced by controlling the carbon precursor adsorption on the catalyst backside [38]. Finally, large area CVD graphene can be easily transferred on a wide variety of substrates [39]. This is of particular interest to decouple the influence of the underlying substrate on the TMD synthesis given graphene's transparency to intermolecular interactions [40].

Up to this day, it remains unclear if graphene is just an atomically smooth inert platform on which TMDs nucleate and grow, if it exhibits any particular catalytic role, and how efficiently it limits the atomic interactions induced by the underlying substrate. The literature does not fully reflect yet how the TMD growth changes when tailoring the graphene thickness, the stacking order/twist angle, and the underlying substrate. Moreover, it is not well understood how graphene attributes (thickness, ripples, wrinkles, ...) influence the adsorption, diffusion, and attachment of ad-atoms, and eventually determine the nucleation and epitaxial relationship between TMDs and graphene.

In this work, we investigate the direct metal–organic chemical vapor deposition (MOCVD) growth of WSe_2 on highly crystalline single-and multi-layer graphene. We conduct a multi-scale investigation of the WSe_2 lattice orientation relatively to the underlying graphene by comparing both the domain edges alignment and electron diffraction patterns. The various factors governing the WSe_2 lattice orientation are discussed and guidelines are provided to minimize the formation of grain boundaries. The number of layers and relative twist angles of graphene are also found to drastically impact the WSe_2 nucleation site density. This study provides a deeper understanding of the mechanisms responsible for the nucleation and growth of WSe_2 crystals and offers valuable insight into ways of controlling thickness, crystallinity, and inplane orientation which are known to determine mechanical, optical, and electronic transport properties.

2. Materials and methods

Graphene synthesis was carried out by chemical vapor deposition in a hot-wall horizontal furnace using methane (1% diluted in Ar) as carbon source and Cu foils (GoodFellow, USA) as catalytic support as described in our previous works [38]. Graphene was then transferred on C-plane sapphire wafers (MSE supplies LLC) with the wet PMMA-assisted transfer method [39]. WSe2 was grown in a coldwall MOCVD reactor using H_2 , tungsten $\mathrm{W(CO)}_6$ and pure $\mathrm{H}_2\mathrm{Se}$ gas. Graphene and WSe2 were observed with a Zeiss Gemini field Emission scanning electron microscope (FE-SEM) using the in-lens detector, an acceleration voltage of about 3 kV, and a working distance ≤4 mm. Raman spectroscopy and photoluminescence (PL) measurements were acquired using an Apyron Confocal Raman Microscope (Witec) with an excitation wavelength of 532 nm, a spot size inferior to 1 micrometer and various gratings ranging from 300 to 1800 gr/mm. Atomic force microscopy (AFM) was conducted using Bruker Dimension Icon with ScanAsyst tips. As-grown WSe2/graphene heterostructures were transferred from sapphire substrates to holey carbon Quantifoil Cu TEM grids with the help of PMMA support layer and NaOH etching solution. The transferred heterostructures are characterized using various TEM characterization techniques such as selected area electron diffraction

(SAED), dark field transmission electron microscopy (DFTEM) imaging and atomic-resolution annular dark field – scanning transmission electron microscopy (ADF – STEM) imaging. SAED and DFTEM imaging are performed using a Thermo Fisher Talos F200X instrument at 80 kV acceleration voltage. Atomic-resolution ADF-STEM imaging is performed using a Thermo Fisher Titan3 G2 microscope equipped with image and probe correctors was operated at 80 kV. The experimental conditions during the ADF-STEM imaging were 30 mrad semi convergence angle and 50 pA screen current. The choice of 80 kV acceleration voltage was to minimize the possible knock-on damage to the samples. Atomic-resolution image in Fig. 3f was filtered using a 2-pixel gaussian blur in the ImageJ program.

3. Results and discussion

3.1. WSe2 synthesis on single layer graphene

Graphene grown by chemical vapor deposition appears to be an ideal synthesis template for studying the nucleation and growth of TMDs. Owing to the significant advances made in the CVD synthesis, highly crystalline graphene with a controlled number of layers can be routinely produced over large areas [36–38] easily transferred onto various substrates compatible with the MOCVD gas precursors and stable at high temperature [20,41].

Large areas of graphene are first grown on Cu foils (6 x 2 in.) in a hot-wall CVD furnace and transferred onto 2 in. C-plane sapphire wafers by the wet PMMA-assisted transfer method [39]. The graphene-coated sapphire wafers are subsequently loaded into the cold-wall MOCVD system. The growth of WSe₂ is carried out at 200 Torr using tungsten hexacarbonyl (W(CO)₆), hydrogen diselenide (H₂Se) and high purity hydrogen as carrier gas. Identical MOCVD conditions were employed throughout the entire investigation unless otherwise noted. Hydrogen diselenide has been preferred to dimethyl selenide (C₂H₆Se) for limiting the incorporation of undesired carbon species in the system [42].

We first investigated the growth of WSe $_2$ on single layer graphene in the 800–1000 °C temperature range with a growth duration set to 12 min (see detailed MOCVD protocol in Supp. Info. 1). Upon exposure to H $_2$ Se and W(CO) $_6$ vapor, triangular WSe $_2$ crystals nucleate, grow and merge together. The size and thickness of these crystals are first assessed by atomic force microscopy (AFM) as shown in Fig. 1a-c. The narrow range of the z scale in the height profiles and the 2D section in Fig. 1c demonstrate that these 2D crystals are mostly single layer. The measured thickness varies in the 0.75 \pm 0.05 nm and 1.4 \pm 0.05 nm ranges for single- and bi-layers, respectively, which is consistent with previous literature [19]. WSe $_2$ crystals were also imaged using scanning electron microscopy (SEM) which is facilitated by the conductive nature of graphene which helps electrons bleeding away from the surface under the beam. Figs. 1d and 1e show the results from a 10 min and a 45 min-long growths carried out at 1000 °C, respectively.

Figs. 1a-c show that the WSe_2 crystal density declines by a factor of about 150 when the susceptor temperature is raised by 200 °C. This observation can be partially attributed to surface-mediated phenomena such as a higher desorption rate of precursors from the surface and an enhanced precursor surface diffusion induced by the increased temperature. It is however challenging to extract the activation energy for the nucleation given that the exact nature of the species that are physisorbed on the substrate has not been well identified yet and the MOCVD gas-phase reactions are complex thermally-activated processes. Moreover, the nucleation site density is found to vary with growth duration, especially in the case of higher temperature growth. For instance, at 1000 °C, figures. 1d-e show that smaller crystals are forming in between the larger crystals due to successive primary, secondary and ternary nucleation events, thus leading to a larger distribution of crystal size (displayed in Fig. 1h).

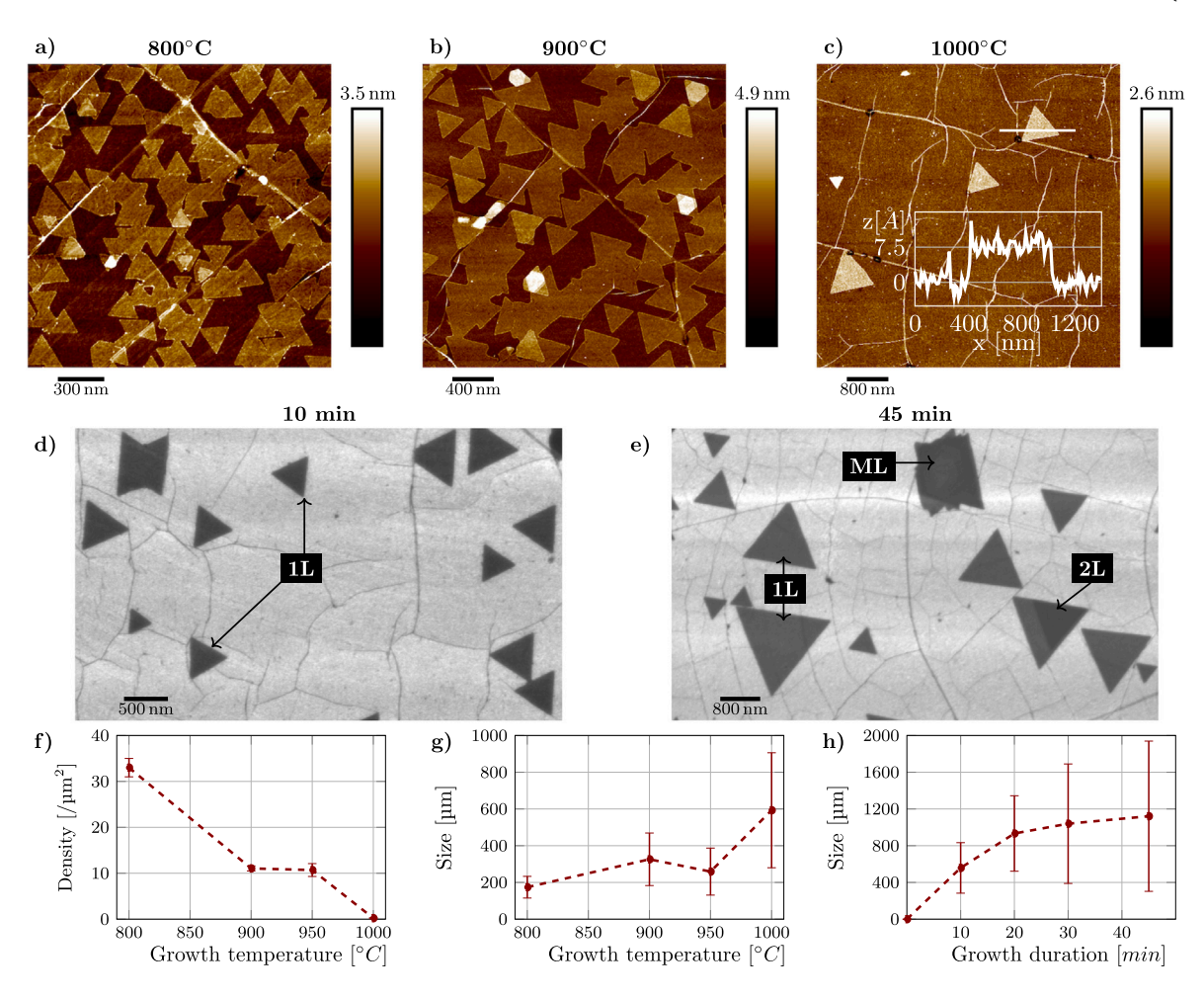


Fig. 1. (a-c) AFM images of WSe₂ grown on graphene (pre-deposited on C-plane sapphire) resulting from the MOCVD 12 min-long MOCVD growth at (a) 800 °C, (b) 900 °C, and (c) 1000 °C. The inlet in (c) shows the 2D high profile corresponding to the white line on the AFM image. (d-e) SEM images of WSe₂ grown on graphene at 1000 °C for (d) 10 min and (e) 45 min. (f-g) Evolution of the nucleation site density and lateral size of WSe₂ crystals as a function of growth temperature. (h) Evolution of the WSe₂ crystal lateral size as a function of growth duration when grown at 1000 °C.

Multiple nucleations usually indicate that adsorbed species prefer to form new nuclei rather than diffusing and attaching to an alreadyexisting crystal. Although this can be indicative of a limited surface diffusion, the consistent well-defined triangular shape, even in the presence of adjacent crystals in the vicinity suggests that the surface diffusion of precursors is not the rate limiting step for the WSe₂ growth. One potential explanation for the multiple nucleations could be that the prolonged exposure of graphene to concentrated hydrogen or WSe₂ precursors could gradually introduce defects in graphene which would then reduce the diffusion or act as preferential sites for nucleation. Although this mechanism has been demonstrated for the growth of WSe2 on h-BN [43], we observed very little or no increase in the D peak intensity in the graphene Raman spectra after the MOCVD process (see details later in this manuscript). Consequently, it does not seem that the multiple nucleations are created by a gradual degradation of graphene during the high temperature process. We however do not exclude the possibility that the smallest domains have been formed during the cooling stage of the MOCVD process when the surface mobility is reduced and remaining precursors are to far from alreadyexisting nuclei. The SEM image in Fig. 1e also shows that long-duration and high-temperature growth promotes the formation of ad-layers, and consequently yield larger thickness variability across the sample. In contrast, a growth temperature of about 800 °C results in a predominantly single layer coalesced film within a relatively short time (about 20 min).

Although graphene wrinkles and ripples typically exhibit an enhanced reactivity due to the out-of-plane deformation and the distortions of the sp² π -bonds [44], graphene wrinkles do not seem to act as preferential sites for WSe₂ nucleation (see supporting information S2). Graphene wrinkles are usually formed either during the graphene growth process due to thermal expansion coefficient (TEC) difference between graphene and the Cu catalyst ($\alpha_{\text{Cu}} \sim 1.8 \times 10^{-5} \text{K}^{-1}$) [37], or during the transfer when the graphene does not properly spread out over the target substrate [39]. These wrinkles typically exhibit higher aspect ratios than those shown in Figs. 1a-e which have been formed after the WSe₂ growth when the MOCVD reactor is cooled down to room temperature due to TEC difference between sapphire and graphene. WSe₂ nucleation does not seem to be impacted by graphene rippling induced by the step bunching of Cu during graphene growth [39,45].

3.2. WSe_2 azimuthal orientation and epitaxy

Qualitatively, AFM and SEM images in Fig. 1 indicate that most WSe_2 crystals follow two preferential orientations rotated by a 60° angle similarly to when it directly grows on sapphire [22]. Such alignment suggests that WSe_2 grows epitaxially either directly with the graphene layer or remotely with the sapphire substrate underneath which exhibit a hexagonal and trigonal symmetries, respectively [41,46]. To elucidate the origin of the epitaxial relationship, we compared the orientation of micrometer-size WSe_2 crystals with the underlying millimeter-size graphene domains (GDs). Adjacent GDs do not systematically exhibit

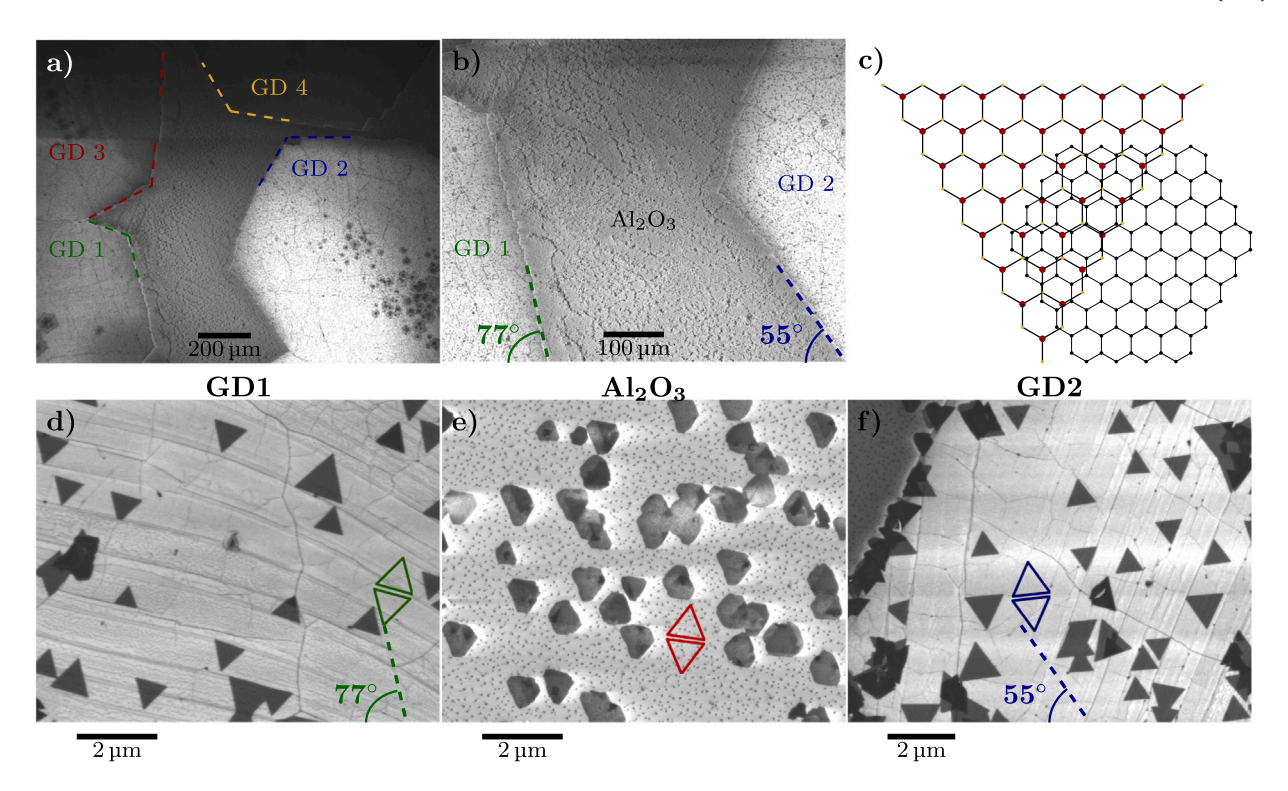


Fig. 2. (a) Large-area SEM image of four hexagonal mm-size graphene domains (GDs) transferred on C-plane sapphire after the MOCVD growth of WSe₂. Higher SEM image of (a) showing the zigzag edge orientation of the graphene domains denoted as GD1 and GD2. (c) Schematic representation of the WSe₂ and graphene lattices and their commensurability. (d), (e), (f) High magnification SEM images taken in GD1, bare sapphire surface and on GD2, respectively.

any in-plane alignment when they are grown on polycrystalline Cu foils and the GD size exceeds the Cu grain size [47,48]. The GD lattice orientation can however be easily estimated from the edge orientation given that hexagon-shaped GDs are usually terminated with zigzag edges which are more stable during the high temperature CVD growth. The large area SEM image in Fig. 2a shows four distinct hexagonal GDs with various orientations as highlighted by the visual guides (dashed colored lines). Fig. 2b shows a higher magnification of the two GDs (referred to as GD1 and GD2) located in the bottom of Fig. 2a. The visual guides show that these two domains are misaligned by an angle of $\sim\!22^\circ.$

SEM images in Figs. 2d, 2e, and 2f were taken on the left graphene domain (as referred to GD1), on bare sapphire, and on the right graphene domain (as referred to GD2), respectively. They clearly show that the azimuthal alignment of WSe2 crystals grown on GD1 differs from those grown on GD2 and on sapphire. It can also be noticed that the zigzag edges of WSe2 are parallel to those of graphene. These observations provide evidence of direct epitaxial growth of WSe₂ with graphene. Lattice matching is usually considered as the main factors driving the azimuthal alignment and epitaxial growth of heterostructures. In the case of van der Waals heterostructures, hexagonal symmetries and long-range commensurability seem to explain the azimuthal alignment of 2D crystals. The lattice constants of WSe2 and graphene unit cells are respectively 3.297 ∀ and 2.46 ∀ which lead to a mismatch of about 33%. The alignment of three WSe2 unit cells on top of four graphene unit cells would lead to very little or no lattice deformation as shown in Fig. 2c. Although comparing the edge orientations of WSe2 and graphene crystals constitutes a rapid and costeffective way of determining the alignment of 2D materials, it does not provide sufficient accuracy for detecting small twisting angles.

To precisely characterize the azimuthal alignment of WSe_2 relative to the graphene lattice using transmission electron microscopy (TEM), the WSe_2 /graphene heterostructures have been transferred onto holey carbon Quantifoil Cu TEM grids [49]. The transfer has been carried out using PMMA as mechanical support for the 2D vdWH and a solution

of NaOH to decouple the heterostructure from the sapphire substrate. Low magnification TEM images in Figs. 3a and 3c show that continuous films of graphene decorated with WSe_2 crystals have been successfully suspended over the 2 micron-size Quantifoil holes.

Fig. 3b displays the selective area electron diffraction (SAED) pattern obtained from the area pointed out by the blue circle in Fig. 3a. The SAED pattern demonstrates the single-crystal nature of WSe₂ and graphene which exhibit a hexagonal symmetry. It also highlights perfect alignment of the WSe2 crystal with graphene, as evidenced by the matching orientations of dashed red and green hexagons, representing the first order reflections of graphene and WSe2, respectively. When the size of the selected area aperture is increased to cover several WSe₂ crystals (as denoted by the blue circle in Fig. 3c), the corresponding SAED pattern indicates that not all WSe2 crystals are perfectly well aligned with graphene. There is a small spread in the distribution of orientations of WSe2 crystals compared to the graphene lattice. Although the small spread could be an artifact caused by the presence of a wrinkle in graphene or by its curvature/deformation when suspended over such a large hole, it does not seem very likely here given that graphene's reflections are much sharper.

Aside from the weak interaction resulting from the vdW stacking, a few other possible reasons could explain the lack of alignment of WSe_2 nuclei when growing on top of graphene. These include (1) thermal fluctuation in graphene due to its 2D nature and the high temperature required for the MOCVD process [50,51], (2) larger lattice mismatch at higher temperature, (3) graphene surface features such as wrinkles and ripples, (4) transfer-induced impurities, and (5) the remote effect from the underlying substrate. Although graphene and WSe_2 exhibit a near perfect commensurability when considering room temperature lattice constants, it is not exactly the case when the actual WSe_2 growth takes place in the 800–1000 °C. The lattice constant (a) can change with temperature (T) as

$$\frac{(a_{gr} - a_0)}{a_0} = \alpha(T)(T_{gr} - T_0),\tag{1}$$

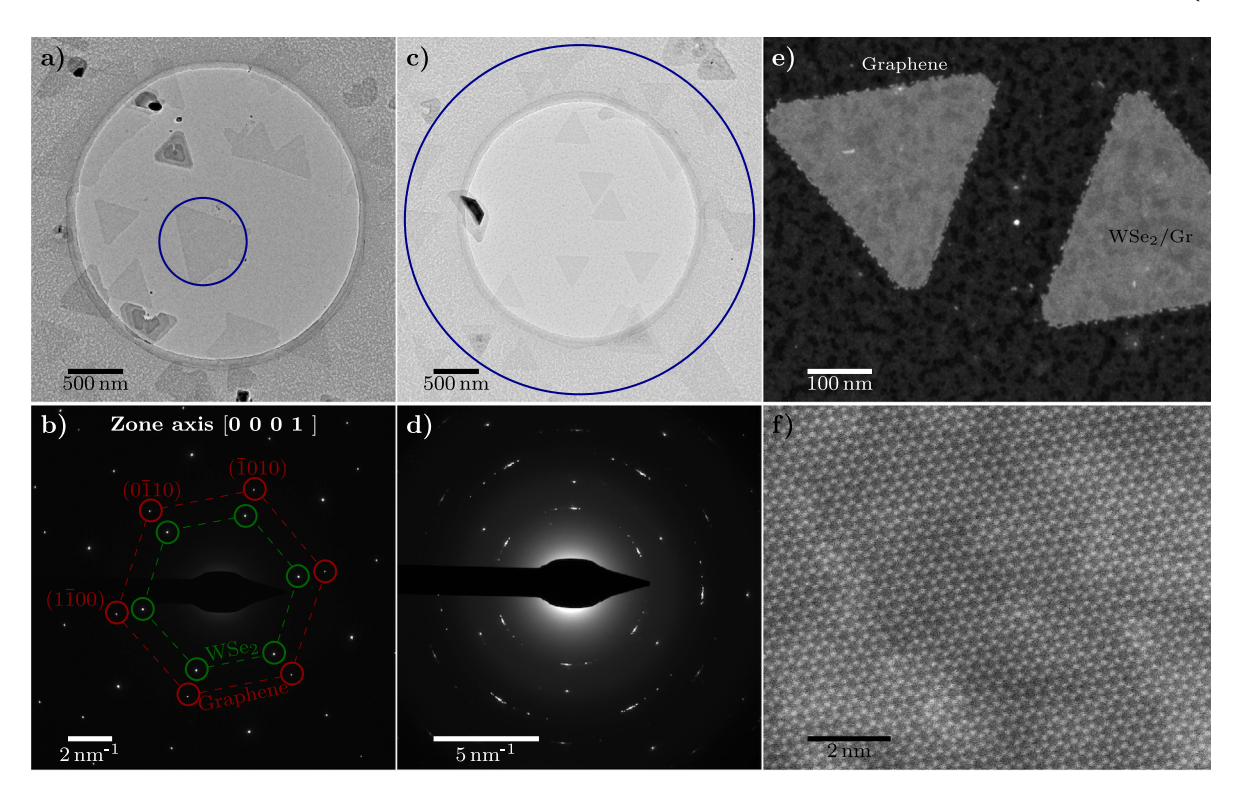


Fig. 3. (a, c) Low magnification TEM images of WSe₂ grown on graphene and transferred onto a TEM grid with a Quantifoil holey carbon film. (b), (d) SAED patterns of graphene and WSe₂ corresponding to the region denoted by the blue circle in (a) and (c), respectively. (e) Low magnification ADF-STEM image of WSe₂ grown on graphene. (f) Atomic-resolution ADF-STEM image of the WSe₂ atomic lattice. (For interpretation of the references to color in this figure legend, the reader is referred to the web version of this article.)

where a_0 and a_{gr} are the lattice constant as the temperature is changed from room temperature T_0 to the MOCVD growth temperature T_{gr} , respectively. Because graphene exhibits a negative TEC (as low as ~2.5 × 10^{-5} K⁻¹) and WSe₂ has a positive TEC (as high as ~ 1.6×10^{-4} K⁻¹) [52], The relative lattice dimension change of the 2D lattices can impede the commensurability and limit the capability of rotation and re-arrangement of WSe2 nuclei. This phenomenon most likely differs from TMD grown on epitaxial graphene which exhibits a more pronounced coupling with the SiC substrate ($\alpha_{\rm SiC} \sim 4.0\times10^{-6}$ K⁻¹) and most likely expands when heated up to the MOCVD growth temperature. Growing TMDs at a lower temperature could thus potentially improve their epitaxial relationship with graphene.

Graphene features like wrinkles and ripples do not seem to play a role in the nucleation of WSe_2 but they are found to disrupt their registry with graphene. WSe_2 crystals are found to align with nanometersize ridges (i.e. the top of the ripples) present in graphene (see Supp. Info S2). When the ridges are close to WSe_2 edges and slightly misaligned, WSe_2 crystals tend to have a zig-zag edge sitting exactly on top of the ridge. It is challenging at this point to determine if this behavior is the result of WSe_2 nuclei rotations before they become too large or if the WSe_2 crystals grow out of this ridges which could act as a barrier for the diffusion and attachment of ad-atoms on the surface. Similar observations were found with WSe_2 crystal aligning with atomic steps of sapphire or with step-edges of SiC when grown on EG/SiC [19,46,53]. In these cases, the alignment has been attributed to the fact that step-edges serve as favorable sites for nucleation and lateral growth across the uphill steps is suppressed.

Annular dark field – scanning transmission electron microscopy (ADF – STEM) has also been performed on the WSe $_2$ /graphene vertical heterostructures. Low magnification image in Fig. 3e shows a rather uniform contrast from the WSe $_2$ crystals sitting on top of graphene layer reflecting the uniform growth of WSe $_2$ and pristine interface. Also, the WSe $_2$ crystals appear brighter compared to the surrounding bare graphene areas owing to the atomic number-contrast mechanism

of the ADF-STEM technique, wherein elements with higher atomic number appear brighter [54]. A careful inspection of several $\rm WSe_2$ centers did not reveal any agglomerates or impurities that could have caused undesired/spurious nucleation. This could potentially rule out the influence of impurities for the lack of complete registry of $\rm WSe_2$ with graphene observed in large area SAED patterns. Atomic resolution image in Fig. 3f shows that there are very little or no defects/vacancies in the WSe $_2$ crystals, which suggest that the selected MOCVD conditions successfully produced high quality vdWHs. The remote effect of the sapphire wafer on the seeding density and azimuthal alignment of WSe $_2$ crystals is discussed in the following section.

3.3. WSe2 growth on multilayer graphene

The growth of WSe2 has also been investigated using highly crystalline multilayer graphene (MLG) as templates. During the graphene CVD synthesis on Cu catalyst, ad-layers typically grow underneath the first growing domain through the diffusion of carbon species from the Cu catalyst bulk to the surface [38]. Due to the polycrystalline nature of the Cu catalyst and the fact that graphene lattice orientation does not strictly match the underlying Cu substrate crystallographic orientation, the top (i.e. the first grown) graphene layer and ad-layers do not systematically exhibit the same in-plane lattice orientation [38]. Fig. 4a shows a SEM image of five crystalline multilayer regions sharing the first top layer. Figs. 4b-c and 4d-e are higher magnification images of MLG domains denoted by the dashed red and green squares in Fig. 4a, respectively. These images show that the two preferential lattice orientations of WSe2 crystals (as illustrated at the bottom of Fig. 4a) remains largely unchanged regardless on the graphene thickness and the multilayer region. This observation suggests that the WSe₂ crystal is primarily dictated by the top graphene layer which is directly sitting underneath. The hexagonal and triangular shapes illustrated at the bottom of Fig. 4a depicts the orientations of the mm-size hexagonal

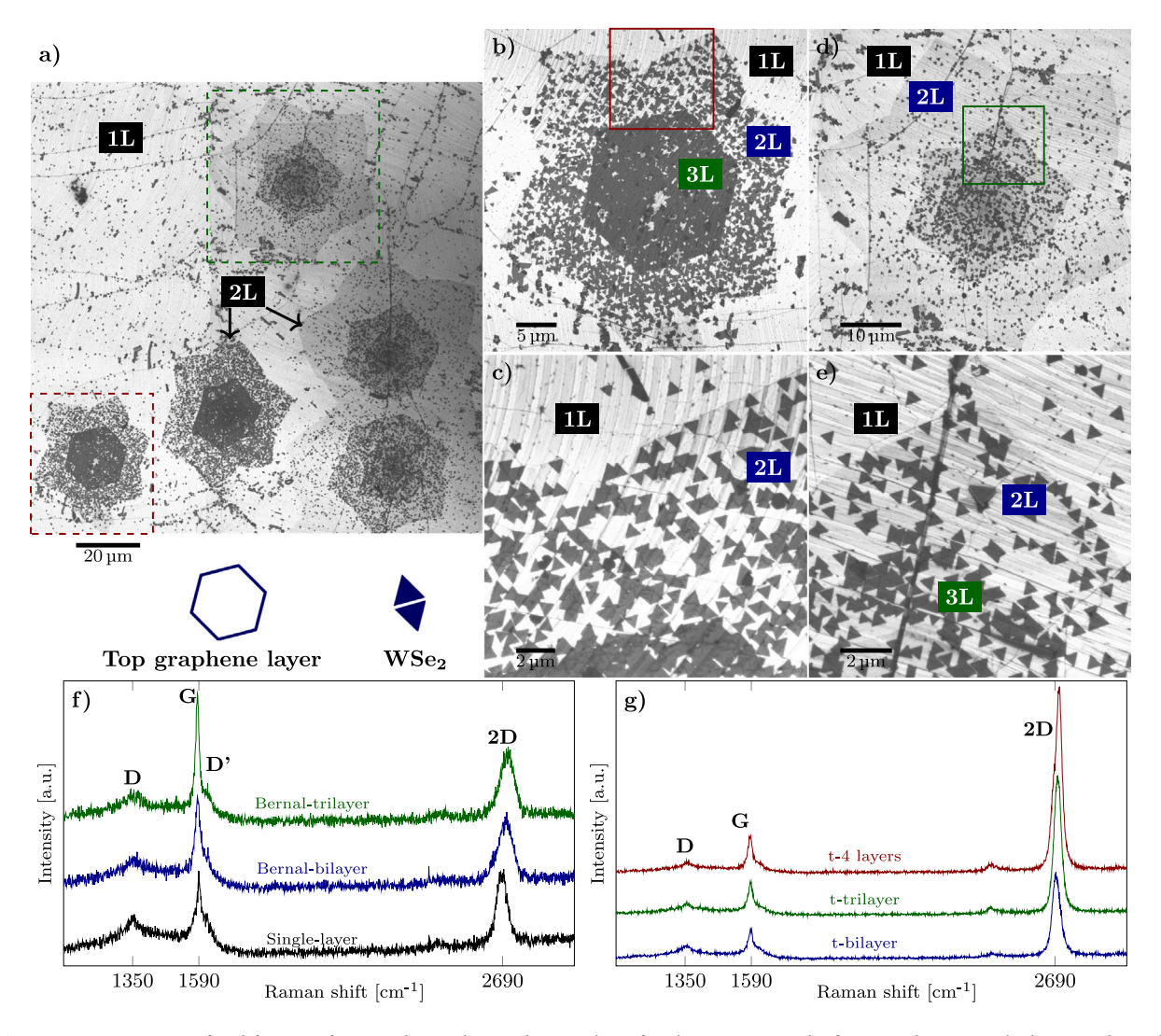


Fig. 4. (a) Large area SEM image of multilayer graphene pre-deposited on C-plane sapphire after the MOCVD growth of WSe2. Schematic at the bottom indicate the lattice orientation of the graphene top layer and the 2 preferential orientation of WSe2 crystals. (b), (d) SEM images of the multilayer graphene regions indicated by the red and green dashed squares in (a). (c), (e) higher magnification SEM images of the solid red and green solid squares in (b) and (d), respectively. (f), (g) Raman spectra of single layer, Bernal-stacked multilayer domain or twisted multilayer domain graphene. (For interpretation of the references to color in this figure legend, the reader is referred to the web version of this article.)

graphene domain (which sits over the add-layers/ML regions) and the epitaxially grown ${\rm WSe}_2$ crystals.

Intuitively, thicker graphene could lead to a better alignment of WSe_2 crystals with graphene top layer since additional graphene layers help screening the polar field induced by the underlying sapphire surface. Additional SEM, AFM and TEM data however show that, qualitatively, a non-negligible fraction of WSe_2 crystals remain misaligned compared to two preferential orientations. This could be due to the presence of graphene ripples which are less frequent but more pronounced in multilayer graphene compared to single-layer graphene [55].

Fig. 4a also shows that the seeding density of WSe $_2$ generally increases with the number of layers. This finding is rather surprising considering that opposite observations were reported when depositing WSe $_2$ on EG/SiC [19]. The increased WSe $_2$ crystal density and rather similar lateral size lead to a much higher WSe $_2$ surface coverage rate. The quasi perfect triangular shape as well as the maintained growth rate indicate that there is a sufficient amount of precursor adsorbed on the surface and precursor surface diffusion is not the rate limiting step.

More interestingly, the WSe₂ seeding density seems to also strongly depend on the graphene stacking order and/or twist angle. The relative

orientation of each graphene layer can be roughly estimated by comparing the edge orientation of each domains. A multilayer graphene stack is generally referred to as AA-stacked when adjacent layers are sitting exactly on top of one another (θ =0°), Bernal-stacked when the layers are parallel-shifted, similarly to the graphite structure, or as twisted multilayer (t-ML) when two adjacent layers are mutually rotated by an angle in the $0^{\circ} < \theta \le 30^{\circ}$ range. WSe₂ crystal density is the highest in the regions where the second and third layers seem to be Bernal-stacked or very slightly misaligned with the first top layer. The other 3 MLG regions in Fig. 4a seem to present a second layer twisted by a $\sim 30^{\circ}$ angle compared to the first and third layers. The twist angle/stacking order is verified by comparing the Raman signatures in various locations as shown in Figs. 4f and 4g. The peak intensity ratio of the 2D (~2690 cm⁻¹) and G (~1590 cm⁻¹) bands, I_{2D}/I_G, is usually greater than 1 for single-layer graphene on sapphire, and gradually decreases as the number of Bernal-stacked layers increases [56]. In contrast, in twisted multilayer graphene, the interlayer electronic coupling drastically decreases with the twist angle, which results in I_{2D}/I_G ratios exceeding 2 for bilayer graphene and even 3 for trilayer graphene [57,58]. More examples of WSe_2 grown on multilayer graphene can be found in Supp. Info. S3.

Considering that the mass transport of gaseous precursor is rather uniform across the substrate surface, it is very likely that the variation of WSe₂ coverage is caused by local variation of surface-mediated phenomena. Graphene's ability to interact with gaseous species and host the WSe₂ growth can be influenced by multiple factors including (i) the presence of structural defects [59], (ii) surface reactivity/charge doping, (iii) surface energy/sticking coefficient [60], (iv) precursor surface diffusivity, (v) mechanical strain in the lattice [61], or even (vi) graphene's ability to screen the ionic field of the underlying substrate [62]. The following discussion aims at unraveling the prominent physical phenomena responsible for the change of WSe₂ with graphene's number of layers and stacking order.

Beside assessing the number of layers and stacking order, Raman spectroscopy can also probe defects, strain and doping in graphene [63]. The peak intensity ratio of the D band (~1350 cm $^{-1}$) and the G band provides a good insight into the density of defects present in the graphene lattice. Figs. 4f-g show that the MOCVD process only causes a very small amount of defects despite the long-duration exposure of graphene to high concentrations of $\rm H_2$ and $\rm H_2Se$ at high temperature. Graphene defects do not seem to be the main factor responsible for the nucleation of WSe $_2$ since the regions with a relatively high $\rm I_D/I_G$ (e.g. single layer graphene) exhibit a relatively low WSe $_2$ density and vice-versa. The rather constant $\rm I_D/I_G$ regardless of the WSe $_2$ surface coverage indicates that sp 3 bonds are not created at the expenses of the graphene sp 2 bonds during WSe $_2$ nucleation and lateral growth, thus corroborating the non-covalent nature of the WSe $_2$ /graphene interlayer interactions.

The absence of chemical reaction between graphene and the precursor vapor suggests that the change of ${\rm WSe}_2$ seeding density is not related to a change of reactivity involving ad-atoms chemisorption and electron transfer chemistries as previously observed with other molecules [64–66].

The drastic change in WSe2 coverage can also be explained by a difference in sticking coefficient which represents the fraction of molecules adsorbing and sticking on the surface compared to the total amount impinging onto it. According to Langmuir adsorption model, the adsorption of species on a surface is limited by the number of adsorption sites. Consequently, a higher number of graphene layers provides an increased number of C atoms that can interact with the gas species and increase the adsorption capability of the surface [67]. The adsorption on bi-, tri- and four-layer graphene should however only vary a little since the field of interaction of the third and fourth layers is drastically limited by their distance from the surface. Compared to twisted multilayer stacks, Bernal-stacked graphene however provides a larger amount of adsorption sites given that atoms of the second layers lie directly in the center of C ring of the first layers. The evolution of adsorption sites thus represents a reasonable explanation to explain the variations of WSe2 coverage observed in Fig. 4.

The sticking coefficient can also be largely governed by other noncovalent interactions that gaseous precursors experience once impinging on graphene. Such binding behavior is intimately correlated to the surface energy and wettability of graphene which are still being debated among the scientific community [60,68,69]. According to the literature, the surface energy/adhesion/wettability depends on adsorbates from the environment (e.g. airborne hydrocarbons, H₂O), polymer residues left behind by the transfer process [70,71], molecules intercalated at the graphene/substrate interface [72], chemical or electrical doping [73,74], the number of graphene layers [68,72], and the type of underlying substrate [40,75,76]. In this case, it is very unlikely that adsorbates, polymer residues or intercalated water molecules would remain to interfere with the WSe2 nucleation since the first step of the MOCVD process consists of a high temperature annealing under 200 Torr of pure hydrogen. It is however very likely that the heat treatment brings graphene in closer contact with the underlying substrate, thus increasing the electrostatic coupling between them and

causing strong charge doping [77]. Precursor molecules landing on graphene are also more prone to experience the electrostatic field of the underlying substrate when the graphene/substrate separation distance is reduced.

To evaluate if the WSe_2 gaseous precursors and adsorbed species are also sensitive to changes of substrate underneath graphene in our experimental conditions, WSe_2 has been grown on CVD graphene predeposited on other substrates including silicon carbide, graphite and h-BN. Optical microscope and SEM images of the resulting WSe_2 growth are shown in Fig. 5 as well as in Supp. Info. S4.

Despite the significant graphene wrinkling and the lack of contrast, a noticeable change in WSe2 density can be observed in Figs. 5c-e. Although this confirms that the underlying substrate plays a role, it remains unclear if the impact of the underlying substrate occurs via polar interaction through graphene, electrostatic doping of graphene, or the introduction of mechanical strain in graphene. Raman spectroscopy measurements show some variations in the position of the G and 2D peaks of graphene, evidencing variations in the electrostatic doping and strain depending on the substrate. Unfortunately, it most likely does not represent the actual strain and doping conditions taking place at 900-1000 °C during the MOCVD growth of WSe₂. Indeed, thermal fluctuations most likely modify the spacing between graphene and the substrate, thus leading to some homogenization of the strain in graphene and weakening the non-covalent electrostatic interactions. Moreover, the high density of wrinkles present in graphene at room temperature on graphite and h-BN were formed during the cooling down process after the WSe2 due to difference in TEC and were not present during the WSe₂ deposition. The presence of high gradients of stress, at smaller or similar scale compared to the Raman spot size, leads to a strong quenching of the intensity of the graphene peaks making it a difficult task to isolate from the substrate contribution.

When comparing the Raman (in Fig. 5g) and photoluminescence (in Fig. 5h) contributions of WSe2 grown on single-, bi- and tri-layer, very little or no difference can be observed. The major difference lies in the increase of signal intensity with the number of graphene layers arising from a larger amount of WSe2 being probe under the 1 micrometerthick laser spot. The absence of the B_{2g} peak (at around 306 cm⁻¹) confirms the single layer nature of the WSe2 crystals/film which was already inferred from the AFM and SEM images. The intense vibration modes E_{2g} and A_{1g} , located respectively at 248 cm⁻¹ and 259 cm⁻¹ are comparable to high quality WSe2 exfoliated or directly synthesized on more conventional substrates such as SiO₂ or sapphire [46,78,79]. The WSe2 photoluminescence signature does not seem to change with the number of graphene layers, thus indicating that WSe2 is under similar levels of strain. Minor variations could however remain inconspicuous because of the relatively low signal-to-noise ratio induced by the strong quenching resulting from the direct contact with graphene and the lack of oxygen and moisture in the glovebox containing the Raman/PL microscope [80,81].

The synthesis of WSe₂ on graphene pre-deposited on SiC also demonstrated a strong evolution of the nucleation site density with the number of graphene layers as observed with sapphire (see Supp. Info. S4). This suggests that the WSe₂ crystal density is governed by the graphene itself rather than a substrate-induced effect that would be increasingly screened with an increasing number of layers.

Finally, to examine the possible role of strain within graphene on WSe $_2$ nucleation density, we employ dark field TEM (DFTEM) imaging. Figs. 6a and 6d display low magnification TEM images of WSe $_2$ /graphene heterostructures formed in monolayer and Bernal stacked bilayer regions of a multilayer graphene domain, respectively. Their corresponding SAED patterns in Figs. 6b and 6e look similar to each other as in they both show only one set of graphene reflections. However, they can be distinguished with the help of intensity ratio of $\{11\bar{2}0\}$ and $\{10\bar{1}0\}$ reflections, as demonstrated in the Supp. Info. S5. DFTEM imaging performed using a $\{10\bar{1}0\}$ graphene reflection (Figs. 6c

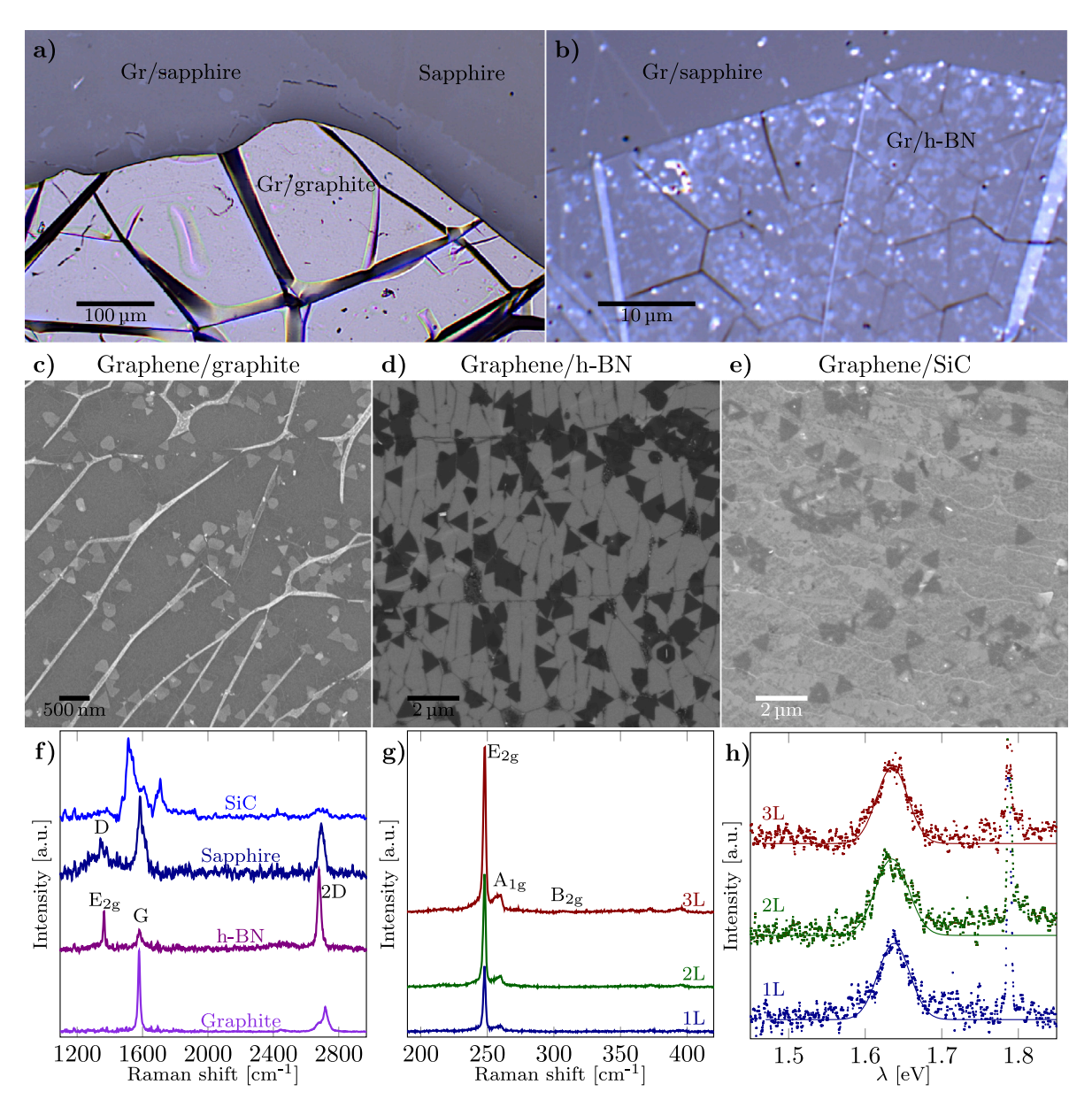


Fig. 5. Optical microscope images of WSe₂ grown on graphene transferred on (a) graphite and (b) h-BN flakes pre-deposited on sapphire. SEM images of WSe₂ grown on graphene transferred on (c) graphite, (d) h-BN, and (e) SiC. (f) Raman Spectra of single-layer graphene on various substrates after the WSe₂ growth. (g) Raman Spectra of WSe₂ grown on single-, bi-, and tri-layer graphene on sapphire. (g) PL spectra of WSe₂ grown on single-, bi-, and tri-layer graphene.

and 6f) clearly show that the Bernal stacked bilayer graphene exhibit strain contrast fluctuations indicating AB to AC stacking changes [82–85], whereas in monolayer graphene no strain contrast is observed. We speculate these stacking changes and the associated strain field could be responsible for the higher nucleation density of WSe₂ crystals in Bernal stacked bilayer graphene and, in general, in multilayer graphene areas. However, further structural and theoretical investigations are needed to confirm the observed correlation. These studies are beyond the scope of this manuscript and will be addressed in a future publication.

4. Conclusions

In summary, we studied the MOCVD growth of tungsten diselenide on top of highly crystalline graphene. The body of experimental data acquired at the micro- and nano-scale provides a deeper understanding of how the WSe₂ growth behavior (nucleation density, growth rate, in-plane orientation, ...) can be influenced by a multitude of factors including the number of graphene layers, their stacking order/twisting

angle, graphene features (ripples, wrinkles, cracks, defects, ...), and even the nature of the underlying substrate. These key findings offer a rationale for engineering and tailoring the growths of vertical 2D heterostructures. The change of WSe_2 crystal density observed when comparing Bernal-stacked and twisted multilayer graphene reveals that graphene does not only serve the role of an inert one-atom thick spacer with an ultra-smooth surface but also displays a novel catalytic role. Although this study only focused on the growth of WSe_2 , it is anticipated that the use of CVD graphene as synthesis scaffold will also contribute to the technological development of vertical heterostructures based on other 2D materials such as WS_2 , $MoSe_2$, and MoS_2 .

CRediT authorship contribution statement

Benjamin Huet: Conceptualization, Methodology, Visualization, Resources, Investigation, Data curation, Writing – original draft. **Saiphaneendra Bachu:** Data curation, Writing – original draft. **Nasim Alem:**

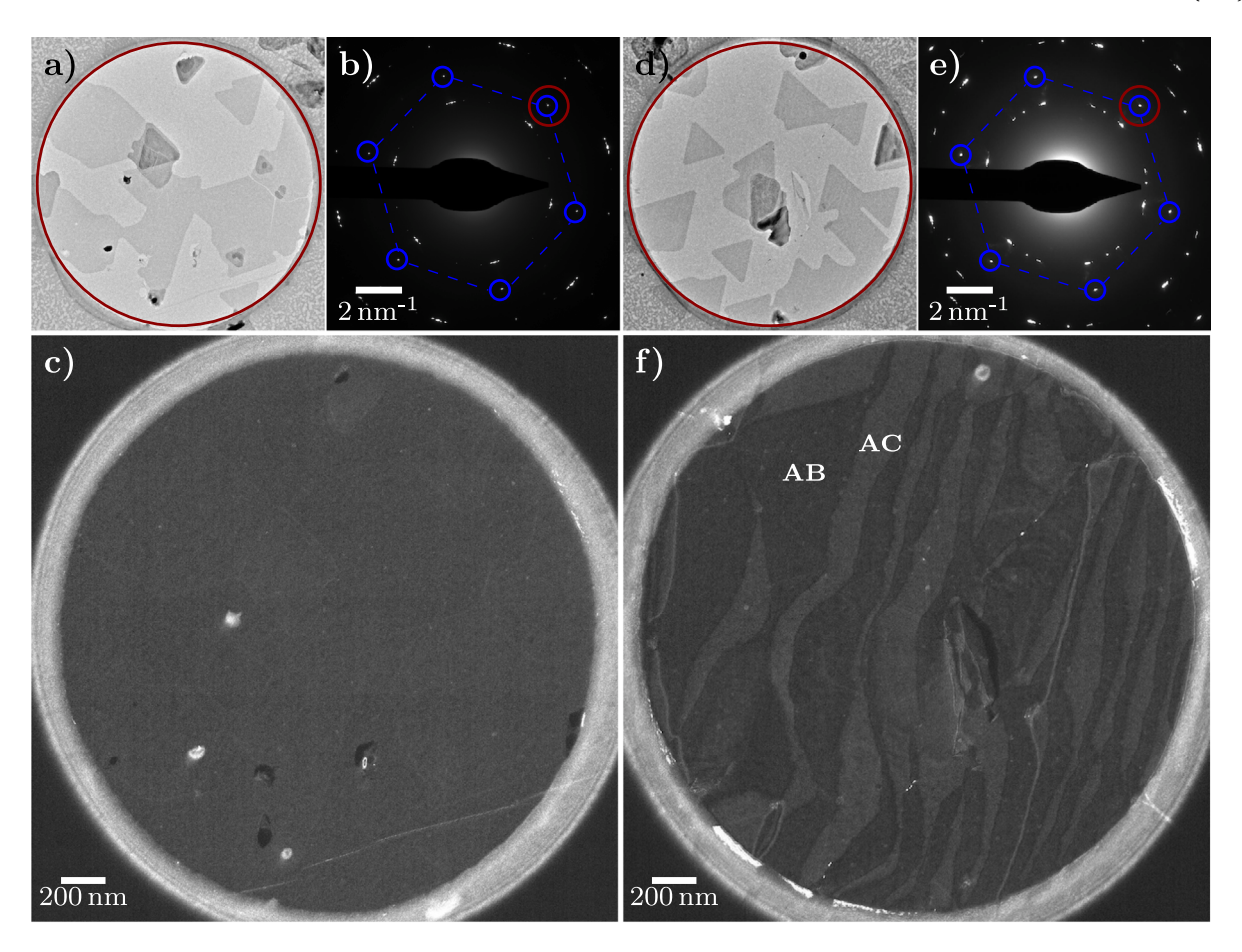


Fig. 6. (a), (d) Low magnification TEM images WSe₂/graphene heterostructures formed in adjacent monolayer and Bernal stacked bilayer regions, respectively. (b), (e) SAED patterns obtained from the red circled regions in (a) and (d), respectively, showing one set of graphene reflections indicated by the blue hexagon. (c), (f) DFTEM images corresponding to (a) and (d) collected by placing the objective aperture around a $\{10\overline{1}0\}$ reflection of graphene (indicated by red circles in (b) and (e)). The strain contrast fluctuations indicating AB to AC stacking changes are only observed in (f) but not in (c). (For interpretation of the references to color in this figure legend, the reader is referred to the web version of this article.)

Reviewing and editing. **David W. Snyder:** Funding acquisition, Reviewing. **Joan M. Redwing:** Funding acquisition, Supervision, Reviewing and editing.

Declaration of competing interest

The authors declare that they have no known competing financial interests or personal relationships that could have appeared to influence the work reported in this paper.

Acknowledgments

The authors acknowledge the financial support of the National Science Foundation (NSF), United States through the Penn State 2D Crystal Consortium – Materials Innovation Platform (2DCC-MIP) under NSF cooperative agreements DMR-1539916 and DMR-2039351. B.H. was also supported by the B.A.E.F. and by the WBI world excellence fellowships for one year at Penn State University. S.B. and N.A. are also grateful for the additional support provided by NSF CAREER DMR-1654107. We gratefully acknowledge the Applied Research Laboratory (ARL), the Nanofabrication Laboratory and the Materials Characterization Lab (MCL) platforms of Penn State University for the CVD and characterization equipment.

Appendix A. Supplementary data

Supplementary material related to this article can be found online at https://doi.org/10.1016/j.carbon.2022.10.037.

References

- [1] Tanushree H. Choudhury, Benjamin Huet, Xiaotian Zhang, Anushka Bansal, Joan M. Redwing, Chapter 1: Scalable Synthesis of 2D materials, in: 2D Materials for Electronics, Sensors and Devices: Synthesis, Characterization, Fabrication and Application, Elsevier, 2022.
- [2] Wouter Mortelmans, Stefan De Gendt, Marc Heyns, Clement Merckling, Epitaxy of 2D chalcogenides: Aspects and consequences of weak van der Waals coupling, Appl. Mater. Today 22 (2021) 100975.
- [3] Qing Hua Wang, Kourosh Kalantar-Zadeh, Andras Kis, Jonathan N. Coleman, Michael S. Strano, Electronics and optoelectronics of two-dimensional transition metal dichalcogenides, Nature Nanotechnol. 7 (2012) 699–712.
- [4] Saptarshi Das, Joerg Appenzeller, WSe2 field effect transistors with enhanced ambipolar characteristics, Appl. Phys. Lett. 103 (10) (2013) 103501.
- [5] Changjian Zhou, Salahuddin Raju, Bin Li, Mansun Chan, Yang Chai, Cary Y. Yang, Self-driven metal?semiconductor?metal WSe2 photodetector with asymmetric contact geometries, Adv. Funct. Mater. 28 (45) (2018) 1802954.
- [6] Guoli Li, Nicolas André, Benjamin Huet, Thibault Delhaye, Nicolas Reckinger, Laurent A Francis, Lei Liao, Jean-Pierre Raskin, Yun Zeng, Denis Flandre, Enhanced ultraviolet photoresponse in a graphene-gated ultra-thin Si-based photodiode, J. Phys. D: Appl. Phys. 52 (24) (2019) 245101.
- [7] Rousan Debbarma, Sanjay K. Behura, Yu Wen, Songwei Che, Vikas Berry, WS2-induced enhanced optical absorption and efficiency in graphene/silicon heterojunction photovoltaic cells, Nanoscale 10 (2018) 20218–20225.
- [8] F. Withers, O. Del Pozo-Zamudio, S. Schwarz, S. Dufferwiel, P.M. Walker, T. Godde, A.P. Rooney, A. Gholinia, C.R. Woods, P. Blake, S.J. Haigh, K. Watanabe, T. Taniguchi, I.L. Aleiner, A.K. Geim, V.I. Falko, A.I. Tartakovskii, K.S. Novoselov, WSe2 light-emitting tunneling transistors with enhanced brightness at room temperature, Nano Lett. 15 (12) (2015) 8223–8228.
- [9] Yuan Liu, Nathan O. Weiss, Xidong Duan, Hung-Chieh Cheng, Yu Huang, Xiangfeng Duan, Van der Waals heterostructures and devices, Nat. Rev. Mater. 1 (2016) 16042.
- [10] A.K. Geim, I.V. Grigorieva, Van der Waals heterostructures, Nature 499 (7459) (2013) 419–425.

[11] Wenjing Zhang, Chih-Piao Chuu, Jing-Kai Huang, Chang-Hsiao Chen, Yung-Huang Tsai, Chi-Te Liang, Yu-Ze Chen, Yu-Lun Chueh, Jr-Hau He, Mei-Yin Chou, Lain-Jong Li, Ultrahigh-gain photodetectors based on atomically thin graphene-MoS2 heterostructures, Sci. Rep. 4 (1) (2014) 3826.

- [12] Hao-Ling Tang, Ming-Hui Chiu, Chien-Chih Tseng, Shih-Hsien Yang, Kuan-Jhih Hou, Sung-Yen Wei, Jing-Kai Huang, Yen-Fu Lin, Chen-Hsin Lien, Lain-Jong Li, Multilayer graphene-WSe2 heterostructures for WSe2 transistors, ACS Nano 11 (12) (2017) 12817–12823.
- [13] Ah-Jin Cho, Min-Kyu Song, Dong-Won Kang, Jang-Yeon Kwon, Two-dimensional WSe2/MoS2 p-n heterojunction-based transparent photovoltaic cell and its performance enhancement by fluoropolymer passivation, ACS Appl. Mater. Interfaces 10 (42) (2018) 35972–35977.
- [14] Marco M. Furchi, Andreas Pospischil, Florian Libisch, Joachim BurgdÄrfer, Thomas Mueller, Photovoltaic effect in an electrically tunable van der Waals heterojunction, Nano Lett. 14 (8) (2014) 4785–4791.
- [15] Fengnian Xia, Han Wang, Di Xiao, Madan Dubey, Ashwin Ramasubramaniam, Two-dimensional material nanophotonics, Nat. Photonics 8 (899–907) (2014) 12.
- [16] C.R. Dean, A.F. Young, I. Meric, C. Lee, L. Wang, S. Sorgenfrei, K. Watanabe, T. Taniguchi, P. Kim, K.L. Shepard, J. Hone, Boron nitride substrates for high-quality graphene electronics, Nature Nanotechnol. 5 (2010) 722–726.
- [17] F. Withers, O. Del Pozo-Zamudio, A. Mishchenko, A.P. Rooney, A. Gholinia, K. Watanabe, T. Taniguchi, S.J. Haigh, A.K. Geim, A.I. Tartakovskii, K.S. Novoselov, Light-emitting diodes by band-structure engineering in van der Waals heterostructures, Nature Mater. 14 (1476–4660) (2015) 301–306.
- [18] Andres Castellanos-Gomez, Michele Buscema, Rianda Molenaar, Vibhor Singh, Laurens Janssen, Herre S J van der Zant, Gary A Steele, Deterministic transfer of two-dimensional materials by all-dry viscoelastic stamping, 2D Mater. 1 (1) (2014) 011002.
- [19] Yu-Chuan Lin, Chih-Yuan S. Chang, Ram Krishna Ghosh, Jie Li, Hui Zhu, Rafik Addou, Bogdan Diaconescu, Taisuke Ohta, Xin Peng, Ning Lu, Moon J. Kim, Jeremy T. Robinson, Robert M Wallace, Theresa S. Mayer, Suman Datta, Lain-Jong Li, Joshua A. Robinson, Atomically thin heterostructures based on single-layer tungsten diselenide and graphene, Nano Lett. 14 (12) (2014) 6936–6941
- [20] Sarah M. Eichfeld, Lorraine Hossain, Yu-Chuan Lin, Aleksander F. Piasecki, Benjamin Kupp, A. Glen Birdwell, Robert A. Burke, Ning Lu, Xin Peng, Jie Li, Angelica Azcatl, Stephen McDonnell, Robert M. Wallace, Moon J. Kim, Theresa S. Mayer, Joan M. Redwing, Joshua A. Robinson, Highly scalable atomically thin WSe2 grown via metal organic chemical vapor deposition, ACS Nano 9 (2) (2015) 2080–2087.
- [21] Stefano Agnoli, Alberto Ambrosetti, Tevfik Onur Mentes, Alessandro Sala, Andrea Locatelli, Pier Luigi Silvestrelli, Mattia Cattelan, Sarah Eichfeld, Donna D. Deng, Joshua A. Robinson, José Avila, Chaoyu Chen, Maria Carmen Asensio, Unraveling the structural and electronic properties at the WSe2-graphene interface for a rational design of van der Waals heterostructures, ACS Appl. Nano Mater. 1 (3) (2018) 1131–1140.
- [22] Amin Azizi, Sarah Eichfeld, Gayle Geschwind, Kehao Zhang, Bin Jiang, Debangshu Mukherjee, Lorraine Hossain, Aleksander F. Piasecki, Bernd Kabius, Joshua A. Robinson, Nasim Alem, Freestanding van der Waals heterostructures of graphene and transition metal dichalcogenides, ACS Nano 9 (5) (2015) 4882-4890
- [23] G.V. Bianco, M. Losurdoa, M.M. Giangregorioa, A. Sacchettia, P. Preteb, N. Loverginec, P. Capezzutoa, G. Brunoa, Direct epitaxial CVD synthesis of tungsten disulfide on epitaxial and CVD graphene, RSC Adv. 5 (2015) 98700–98708.
- [24] Stiven Forti, Antonio Rossi, Holger Buch, Tommaso Cavallucci, Francesco Bisio, Alessandro Sala, Tevfik Onur Mentes, Andrea Locatelli, Michele Magnozzi, Maurizio Canepa, Kathrin Muller, Stefan Link, Ulrich Starke, Valentina Tozzini, Camilla Coletti, Electronic properties of single-layer tungsten disulfide on epitaxial graphene on silicon carbide, Nanoscale 9 (2017) 16412–16419.
- [25] Changxi Zheng, Qianhui Zhang, Bent Weber, Hesameddin Ilatikhameneh, Fan Chen, Harshad Sahasrabudhe, Rajib Rahman, Shiqiang Li, Zhen Chen, Jack Hellerstedt, Yupeng Zhang, Wen Hui Duan, Qiaoliang Bao, Michael S. Fuhrer, Direct observation of 2D electrostatics and ohmic contacts in template-grown graphene/WS2 heterostructures, ACS Nano 11 (3) (2017) 2785–2793.
- [26] Holger Büch, Antonio Rossi, Stiven Forti, Domenica Convertino, Valentina Tozzini, Camilla Coletti, Superlubricity of epitaxial monolayer WS2 on graphene, Nano Res. 11 (11) (2018) 5946–5956.
- [27] Chendong Zhang, Amber Johnson, Chang-Lung Hsu, Lain-Jong Li, Chih-Kang Shih, Direct imaging of band profile in single layer MoS2 on graphite: Quasiparticle energy gap, metallic edge states, and edge band bending, Nano Lett. 14 (5) (2014) 2443–2447.
- [28] Yu-Chuan Lin, Ning Lu, Nestor Perea-Lopez, Jie Li, Zhong Lin, Xin Peng, Chia Hui Lee, Ce Sun, Lazaro Calderin, Paul N. Browning, Michael S. Bresnehan, Moon J. Kim, Theresa S. Mayer, Mauricio Terrones, Joshua A. Robinson, Direct synthesis of van der Waals solids, ACS Nano 8 (4) (2014) 3715–3723.
- [29] Chun-I Lu, Christopher John Butler, Jing-Kai Huang, Cheng-Rong Hsing, Hung-Hsiang Yang, Yu-Hsun Chu, Chi-Hung Luo, Yung-Che Sun, Shih-Hao Hsu, Kui-Hong Ou Yang, Ching-Ming Wei, Lain-Jong Li, Minn-Tsong Lin, Graphite edge controlled registration of monolayer MoS2 crystal orientation, Appl. Phys. Lett. 106 (18) (2015) 181904.

[30] Jill A. Miwa, Maciej Dendzik, Signe S. Gronborg, Marco Bianchi, Jeppe V. Lauritsen, Philip Hofmann, Soren Ulstrup, Van der Waals epitaxy of two-dimensional MoS2-graphene heterostructures in ultrahigh vacuum, ACS Nano 9 (6) (2015) 6502–6510.

- [31] Yu-Chuan Lin, Bhakti Jariwala, Brian M. Bersch, Ke Xu, Yifan Nie, Baoming Wang, Sarah M. Eichfeld, Xiaotian Zhang, Tanushree H. Choudhury, Yi Pan, Rafik Addou, Christopher M. Smyth, Jun Li, Kehao Zhang, M. Aman Haque, Stefan FÃlsch, Randall M. Feenstra, Robert M. Wallace, Kyeongjae Cho, Susan K. Fullerton-Shirey, Joan M. Redwing, Joshua A. Robinson, Realizing large-scale, electronic-grade two-dimensional semiconductors, ACS Nano 12 (2) (2018) 965–975.
- [32] Xiaotian Zhang, Tanushree H. Choudhury, Mikhail Chubarov, Yu Xiang, Bhakti Jariwala, Fu Zhang, Nasim Alem, Gwo-Ching Wang, Joshua A. Robinson, Joan M. Redwing, Diffusion-controlled epitaxy of large area coalesced WSe2 monolayers on sapphire, Nano Lett. 18 (2) (2018) 1049–1056.
- [33] Tanushree H. Choudhury, Hamed Simchi, RaphaÃl Boichot, Mikhail Chubarov, Suzanne E. Mohney, Joan M. Redwing, Chalcogen precursor effect on cold-wall gas-source chemical vapor deposition growth of WS2, Cryst. Growth Des. 18 (8) (2018) 4357–4364.
- [34] Kai-Ge Zhou, Freddie Withers, Yang Cao, Sheng Hu, Geliang Yu, Cinzia Casiraghi, Raman modes of MoS2 used as fingerprint of van der Waals interactions in 2-D crystal-based heterostructures, ACS Nano 8 (10) (2014) 9914–9924.
- [35] Benjamin Huet, Jean-Pierre Raskin, Pressure-controlled chemical vapor deposition of single-layer graphene with millimeter-size domains on thin copper film, Chem. Mater. 29 (2017) 3431–3440.
- [36] Benjamin Huet, Xiaotian Zhang, Joan M Redwing, David W. Snyder, Jean-Pierre Raskin, Multi-wafer batch synthesis of graphene on Cu films by quasi-static flow chemical vapor deposition, 2D Mater. 6 (4) (2019) 045032.
- [37] Benjamin Huet, Jean-Pierre Raskin, Role of the Cu substrate in the growth of ultra-flat crack-free highly-crystalline single-layer graphene, Nanoscale 10 (2018) 21898–21909.
- [38] Benjamin Huet, Jean-Pierre Raskin, Role of Cu foil in-situ annealing in controlling the size and thickness of CVD graphene domains, Carbon 129 (2018) 270–280.
- [39] Benjamin Huet, Jean-Pierre Raskin, David W. Snyder, Joan M. Redwing, Fundamental limitations in transferred CVD graphene caused by Cu catalyst surface morphology, Carbon 163 (2020) 95–104.
- [40] Wei Kong, Huashan Li, Kuan Qiao, Yunjo Kim, Kyusang Lee, Yifan Nie, Doyoon Lee, Tom Osadchy, Richard J. Molnar, Rachael L. Gaskill, Kevin M. Daniels, Yuewei Zhang, Suresh Sundram, Yang Yu, Sang-hoon Bae, Siddharth Rajan, Yang Shao-Horn, Kyeongjae Cho, Abdallah Ougazzaden, Jeffrey C. Grossman, Jeehwan Kim, Polarity governs atomic interaction through two-dimensional materials, Nature Mater. 17 (11) (2018) 999–1004.
- [41] Anushka Bansal, Maria Hilse, Benjamin Huet, Ke Wang, Azimkhan Kozhakhmetov, Ji Hyun Kim, Saiphaneendra Bachu, Nasim Alem, Ramon Collazo, Joshua A. Robinson, Roman Engel-Herbert, Joan M. Redwing, Substrate modification during chemical vapor deposition of hBN on sapphire, ACS Appl. Mater. Interfaces 13 (45) (2021) 54516–54526.
- [42] Xiaotian Zhang, Zakaria Y. Al Balushi, Fu Zhang, Tanushree H. Choudhury, Sarah M. Eichfeld, Nasim Alem, Thomas N. Jackson, Joshua A. Robinson, Joan M. Redwing, Influence of carbon in metalorganic chemical vapor deposition of few-layer WSe2 thin films, J. Electron. Mater. 45 (2016) 6273–6279.
- [43] Xiaotian Zhang, Fu Zhang, Yuanxi Wang, Daniel S. Schulman, Tianyi Zhang, Anushka Bansal, Nasim Alem, Saptarshi Das, Vincent H. Crespi, Mauricio Terrones, Joan M. Redwing, Defect-controlled nucleation and orientation of WSe2 on hBN: A route to single-crystal epitaxial monolayers, ACS Nano 13 (3) (2019) 3341–3352.
- [44] Yanhong Zhang, Qiang Fu, Yi Cui, Rentao Mu, Li Jin, Xinhe Bao, Enhanced reactivity of graphene wrinkles and their function as nanosized gas inlets for reactions under graphene, Phys. Chem. Chem. Phys. 15 (2013) 19042–19048.
- [45] Guang-Xin Ni, Yi Zheng, Sukang Bae, Hye Ri Kim, Alexandre Pachoud, Young Soo Kim, Chang-Ling Tan, Danho Im, Jong-Hyun Ahn, Byung Hee Hong, Barbaros Azyilmaz, Quasi-periodic nanoripples in graphene grown by chemical vapor deposition and its impact on charge transport, ACS Nano 6 (2) (2012) 1158–1164.
- [46] Xuegang Chen, Benjamin Huet, Tanushree H. Choudhury, Joan M. Redwing, Toh-Ming Lu, Gwo-Ching Wang, Orientation domain dispersions in wafer scale epitaxial monolayer WSe2 on sapphire, Appl. Surf. Sci. 567 (2021) 150798.
- [47] Adrian T. Murdock, Antal Koos, T. Ben Britton, Lothar Houben, Tim Batten, Tong Zhang, Angus J. Wilkinson, Rafal E. Dunin-Borkowski, Christina E. Lekka, Nicole Grobert, Controlling the orientation, edge geometry, and thickness of chemical vapor deposition graphene, ACS Nano 7 (2013) 1351–1359.
- [48] Yuting Hou, Bojun Wang, Longlong Zhan, Fangzhu Qing, Xiaomu Wang, Xiaobin Niu, Xuesong Li, Surface crystallographic structure insensitive growth of oriented graphene domains on Cu substrates, Mater. Today (2020).
- [49] Saiphaneendra Bachu, Benjamin Huet, Danielle Reifsnyder Hickey, Chenhao Qian, Joan Redwing, Nasim Alem, S/TEM characterization of vertical heterostructures formed by mono- to multi-layer graphene and WSe2, Microsc. Microanal. 27 (S1) (2021) 894–895.

[50] P. Xu, M. Neek-Amal, S.D. Barber, J.K. Schoelz, M.L. Ackerman, P.M. Thibado, A. Sadeghi, F.M. Peeters, Unusual ultra-low-frequency fluctuations in freestanding graphene. Nature Commun. 5 (1) (2014) 3720.

- [51] Hiroki Ago, Yujiro Ohta, Hiroki Hibino, Daisuke Yoshimura, Rina Takizawa, Yuki Uchida, Masaharu Tsuji, Toshihiro Okajima, Hisashi Mitani, Seigi Mizuno, Growth dynamics of single-layer graphene on epitaxial Cu surfaces, Chem. Mater. 27 (2015) 5377–5385.
- [52] Xuan Hu, Poya Yasaei, Jacob Jokisaari, Serdar Öğüt, Amin Salehi-Khojin, Robert F. Klie, Mapping thermal expansion coefficients in freestanding 2D materials at the nanometer scale, Phys. Rev. Lett. 120 (2018) 055902.
- [53] Liang Chen, Bilu Liu, Mingyuan Ge, Yuqiang Ma, Ahmad N. Abbas, Chongwu Zhou, Step-edge-guided nucleation and growth of aligned WSe2 on sapphire via a layer-over-layer growth mode, ACS Nano 9 (8) (2015) 8368–8375.
- [54] Ondrej L Krivanek, Matthew F Chisholm, Valeria Nicolosi, Timothy J Pennycook, George J Corbin, Niklas Dellby, Matthew F Murfitt, Christopher S Own, Zoltan S Szilagyi, Mark P Oxley, Sokrates T Pantelides, Stephen J Pennycook, Atom-byatom structural and chemical analysis by annular dark-field electron microscopy, Nature 464 (7288) (2010) 571–574.
- [55] Ding Yi, Da Luo, Zhu-Jun Wang, Jichen Dong, Xu Zhang, Marc-Georg Willinger, Rodney S. Ruoff, Feng Ding, What drives metal-surface step bunching in graphene chemical vapor deposition? Phys. Rev. Lett. 120 (2018) 246101.
- [56] Kiran M. Subhedar, Indu Sharma, Sanjay R. Dhakate, Control of layer stacking in CVD graphene under quasi-static condition, Phys. Chem. Chem. Phys. 17 (2015) 22304–22310.
- [57] Kwanpyo Kim, Sinisa Coh, Liang Z. Tan, William Regan, Jong Min Yuk, Eric Chatterjee, M.F. Crommie, Marvin L. Cohen, Steven G. Louie, A. Zettl, Raman spectroscopy study of rotated double-layer graphene: Misorientation-angle dependence of electronic structure, Phys. Rev. Lett. 108 (2012) 246103.
- [58] Yen-Chun Chen, Wei-Hsiang Lin, Wei-Shiuan Tseng, Chien-Chang Chen, George R. Rossman, Chii-Dong Chen, Yu-Shu Wu, Nai-Chang Yeh, Direct growth of mm-size twisted bilayer graphene by plasma-enhanced chemical vapor deposition, Carbon 156 (2020) 212–224.
- [59] Surya Nalamati, Shisir Devkota, Jia Li, Robert Lavelle, Benjamin Huet, David Snyder, Aubrey Penn, Roberto Garcia, Lewis Reynolds, Shanthi Iyer, Hybrid GaAsSb/GaAs heterostructure core-shell nanowire/graphene and photodetector applications, ACS Appl. Electron. Mater. 2 (10) (2020) 3109–3120.
- [60] Wouter Mortelmans, Ankit Nalin Mehta, Yashwanth Balaji, Stefanie Sergeant, Ruishen Meng, Michel Houssa, Stefan De Gendt, Marc Heyns, Clement Merckling, On the van der Waals epitaxy of homo-/heterostructures of transition metal dichalcogenides, ACS Appl. Mater. Interfaces 12 (24) (2020) 27508–27517.
- [61] Mark A. Bissett, Satoru Konabe, Susumu Okada, Masaharu Tsuji, Hiroki Ago, Enhanced chemical reactivity of graphene induced by mechanical strain, ACS Nano 7 (11) (2013) 10335–10343.
- [62] Timothy Mirabito, Benjamin Huet, Joan M. Redwing, David W. Snyder, Influence of the underlying substrate on the physical vapor deposition of Zn-phthalocyanine on graphene, ACS Omega 6 (31) (2021) 20598–20610.
- [63] Andrea C. Ferrari, Denis M. Basko, Raman spectroscopy as a versatile tool for studying the properties of graphene, Nat. Nano 8 (2013) 235–246.
- [64] Richa Sharma, Joon Hyun Baik, Chrisantha J. Perera, Michael S. Strano, Anomalously large reactivity of single graphene layers and edges toward electron transfer chemistries, Nano Lett. 10 (2) (2010) 398–405.
- [65] Yao Ding, Qing Peng, Lin Gan, Ruizhe Wu, Xuewu Ou, Qicheng Zhang, Zhengtang Luo, Stacking-mode-induced reactivity enhancement for twisted bilayer graphene, Chem. Mater. 28 (4) (2016) 1034–1039.
- [66] Myung Jin Park, Hae-Hyun Choi, Baekwon Park, Jae Yoon Lee, Chul-Ho Lee, Yong Seok Choi, Youngsoo Kim, Je Min Yoo, Hyukjin Lee, Byung Hee Hong, Enhanced chemical reactivity of graphene by Fermi level modulation, Chem. Mater. 30 (16) (2018) 5602–5609.
- [67] Chengzhen Sun, Bofeng Bai, Diffusion of gas molecules on multilayer graphene surfaces: Dependence on the number of graphene layers, Appl. Therm. Eng. 116 (2017) 724–730.
- [68] Christian D. van Engers, Nico E.A. Cousens, Vitaliy Babenko, Jude Britton, Bruno Zappone, Nicole Grobert, Susan Perkin, Direct measurement of the surface energy of graphene, Nano Lett. 17 (6) (2017) 3815–3821.

- [69] Filchito Renee Bagsican, Andrew Winchester, Sujoy Ghosh, Xiang Zhang, Lulu Ma, Minjie Wang, Hironaru Murakami, Saikat Talapatra, Robert Vajtai, Pulickel M. Ajayan, Junichiro Kono, Masayoshi Tonouchi, Iwao Kawayama, Adsorption energy of oxygen molecules on graphene and two-dimensional tungsten disulfide, Sci. Rep. 7 (1) (2017) 1774.
- [70] Zhiting Li, Yongjin Wang, Andrew Kozbial, Ganesh Shenoy, Feng Zhou, Rebecca McGinley, Patrick Ireland, Brittni Morganstein, Alyssa Kunkel, Sumedh P. Surwade, Lei Li, Haitao Liu, Effect of airborne contaminants on the wettability of supported graphene and graphite, Nature Mater. 12 (10) (2013) 925–931.
- [71] Chia-Yun Lai, Tzu-Chieh Tang, Carlo A. Amadei, Alexander J. Marsden, Albert Verdaguer, Neil Wilson, Matteo Chiesa, A nanoscopic approach to studying evolution in graphene wettability, Carbon 80 (2014) 784–792.
- [72] Jin-You Lu, Tuza Olukan, Srinivasa Reddy Tamalampudi, Abdulrahman Al-Hagri, Chia-Yun Lai, Mariam Ali Al Mahri, Harry Apostoleris, Ibraheem Almansouri, Matteo Chiesa, Insights into graphene wettability transparency by locally probing its surface free energy, Nanoscale 11 (2019) 7944–7951.
- [73] Felix Huttmann, Antonio J. Martínez-Galera, Vasile Caciuc, Nicolae Atodiresei, Stefan Schumacher, Sebastian Standop, Ikutaro Hamada, Tim O. Wehling, Stefan Blügel, Thomas Michely, Tuning the van der Waals interaction of graphene with molecules via doping, Phys. Rev. Lett. 115 (2015) 236101.
- [74] Guo Hong, Yang Han, Thomas M. Schutzius, Yuming Wang, Ying Pan, Ming Hu, Jiansheng Jie, Chander S. Sharma, Ulrich Müller, Dimos Poulikakos, On the mechanism of hydrophilicity of graphene, Nano Lett. 16 (7) (2016) 4447–4453.
- [75] Feng Du, Jianyong Huang, Huiling Duan, Chunyang Xiong, Jianxiang Wang, Wetting transparency of supported graphene is regulated by polarities of liquids and substrates, Appl. Surf. Sci. 454 (2018) 249–255.
- [76] Javad Rafiee, Xi Mi, Hemtej Gullapalli, Abhay V. Thomas, Fazel Yavari, Yunfeng Shi, Pulickel M. Ajayan, Nikhil A. Koratkar, Wetting transparency of graphene, Nature Mater. 11 (3) (2012) 217–222.
- [77] Zengguang Cheng, Qiaoyu Zhou, Chenxuan Wang, Qiang Li, Chen Wang, Ying Fang, Toward intrinsic graphene surfaces: A systematic study on thermal annealing and wet-chemical treatment of SiO2-supported graphene devices, Nano Lett. 11 (2) (2011) 767–771.
- [78] Jing-Kai Huang, Jiang Pu, Chang-Lung Hsu, Ming-Hui Chiu, Zhen-Yu Juang, Yung-Huang Chang, Wen-Hao Chang, Yoshihiro Iwasa, Taishi Takenobu, Lain-Jong Li, Large-area synthesis of highly crystalline WSe2 monolayers and device applications, ACS Nano 8 (1) (2014) 923–930.
- [79] Bilu Liu, Mohammad Fathi, Liang Chen, Ahmad Abbas, Yuqiang Ma, Chongwu Zhou, Chemical vapor deposition growth of monolayer WSe2 with tunable device characteristics and growth mechanism study, ACS Nano 9 (6) (2015) 6119–6127.
- [80] Bowen Yang, Everardo Molina, Jeongwoo Kim, David Barroso, Mark Lohmann, Yawen Liu, Yadong Xu, Ruqian Wu, Ludwig Bartels, Kenji Watanabe, Takashi Taniguchi, Jing Shi, Effect of distance on photoluminescence quenching and proximity-induced spin-orbit coupling in graphene/WSe2 heterostructures, Nano Lett. 18 (6) (2018) 3580-3585.
- [81] Blake Birmingham, Jiangtan Yuan, Matthias Filez, Donglong Fu, Jonathan Hu, Jun Lou, Marlan O. Scully, Bert M. Weckhuysen, Zhenrong Zhang, Spatially-resolved photoluminescence of monolayer MoS2 under controlled environment for ambient optoelectronic applications, ACS Appl. Nano Mater. 1 (11) (2018) 6226–6235.
- [82] Jonathan S. Alden, Adam W. Tsen, Pinshane Y. Huang, Robert Hovden, Lola Brown, Jiwoong Park, David A. Muller, Paul L. McEuen, Strain solitons and topological defects in bilayer graphene, Proc. Natl. Acad. Sci. 110 (28) (2013) 11256–11260.
- [83] Junhao Lin, Wenjing Fang, Wu Zhou, Andrew R. Lupini, Juan Carlos Idrobo, Jing Kong, Stephen J. Pennycook, Sokrates T. Pantelides, AC/AB stacking boundaries in bilayer graphene, Nano Lett. 13 (7) (2013) 3262–3268.
- [84] Benjamin Butz, Christian Dolle, Florian Niekiel, Konstantin Weber, Daniel Waldmann, Heiko B Weber, Bernd Meyer, Erdmann Spiecker, Dislocations in bilayer graphene, Nature 505 (7484) (2014) 533–537.
- [85] Lola Brown, Robert Hovden, Pinshane Huang, Michal Wojcik, David A. Muller, Jiwoong Park, Twinning and twisting of tri- and bilayer graphene, Nano Lett. 12 (3) (2012) 1609–1615.